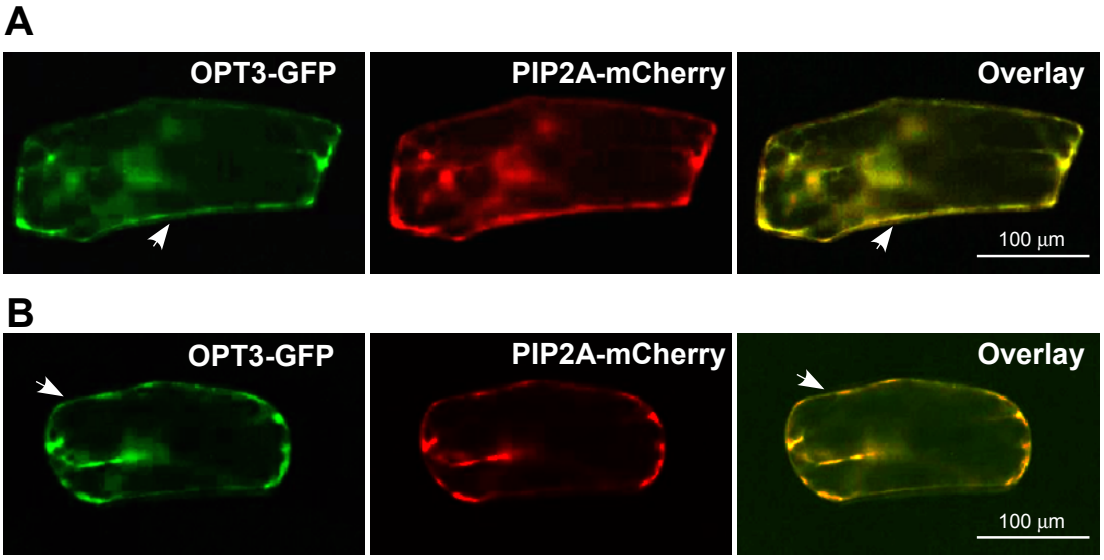

Supplemental Figure 1 online. OPT3-GFP localizes to the plasma membrane in epidermal onion cells. A. Onion cells were co-transformed with OPT3 fused to GFP (**OPT3-GFP**) and a plasma membrane marker, PIP2A, fused to mCherry (**PIP2A-mCherry**). **B.** Onion cells transiently co-expressing OPT3-GFP and PIP2A-mCherry were plasmolyzed in 20% sucrose solution for 10 min before imaging. GFP- and mCherry-mediated fluorescence was visualized using FITC and Rhodamine filter sets respectively. Arrows point to plasma membrane localization of OPT3-GFP. Superimposed images (**Overlay**) of OPT3-GFP- and PIP2A-mCherry-mediated fluorescence were generated to demonstrate the co-localization of OPT3-GFP with PIP2A-mCherry (**A** and **B**).

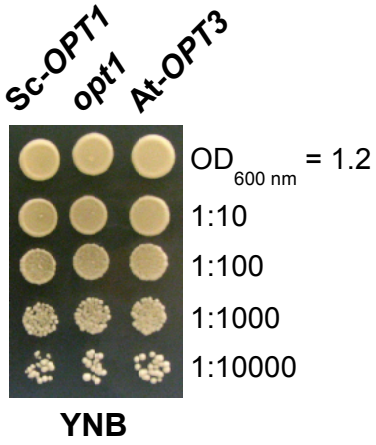

Supplemental Figure 2 online. *OPT3* does not alter growth of the *opt1* mutant of *S. cerevisiae* under control conditions. *S. cerevisiae opt1* mutant cells expressing Sc-*OPT1* cDNA ***(Sc-OPT1)***, the empty vector (***opt1***) or the vector with the At-*OPT3* cDNA insert (**At-*OPT3***) were grown in liquid YNB media overnight to an OD_{600nm} of 1.2. Cells were then serially 10-fold diluted and spotted onto solid YNB medium. Colonies were visualized after incubating plates for 3 days at 30°C. Dilution series are indicated on the left.

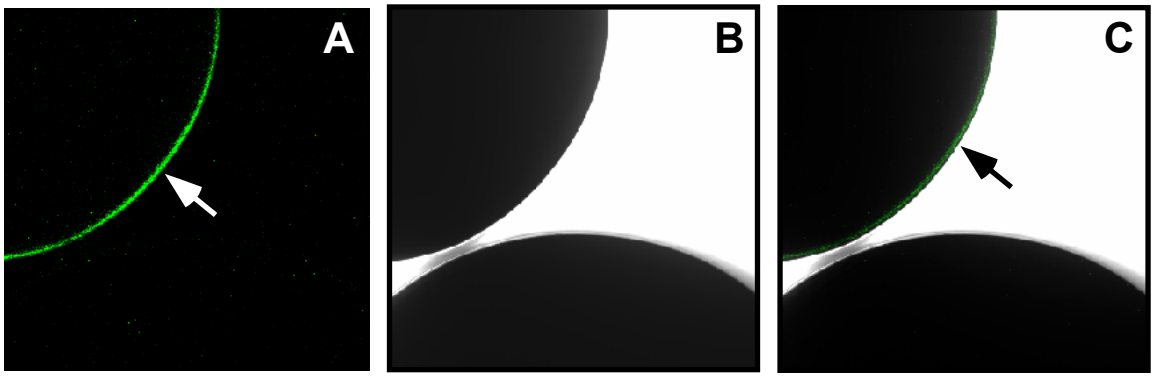

Supplemental Figure 3 online. OPT3 localizes to the plasma membrane in *X. laevis* oocytes. The fluorescence signal from the OPT3-EGFP chimera expressed in *X. laevis* oocytes (upper cell) was localized to the plasma membrane (arrow) (**A**). Water-injected cells showed no fluorescence background signal (lower cell). Images illustrate fluorescence image (**A**), the corresponding bright field image (**B**), and the overlay of both images (**C**).

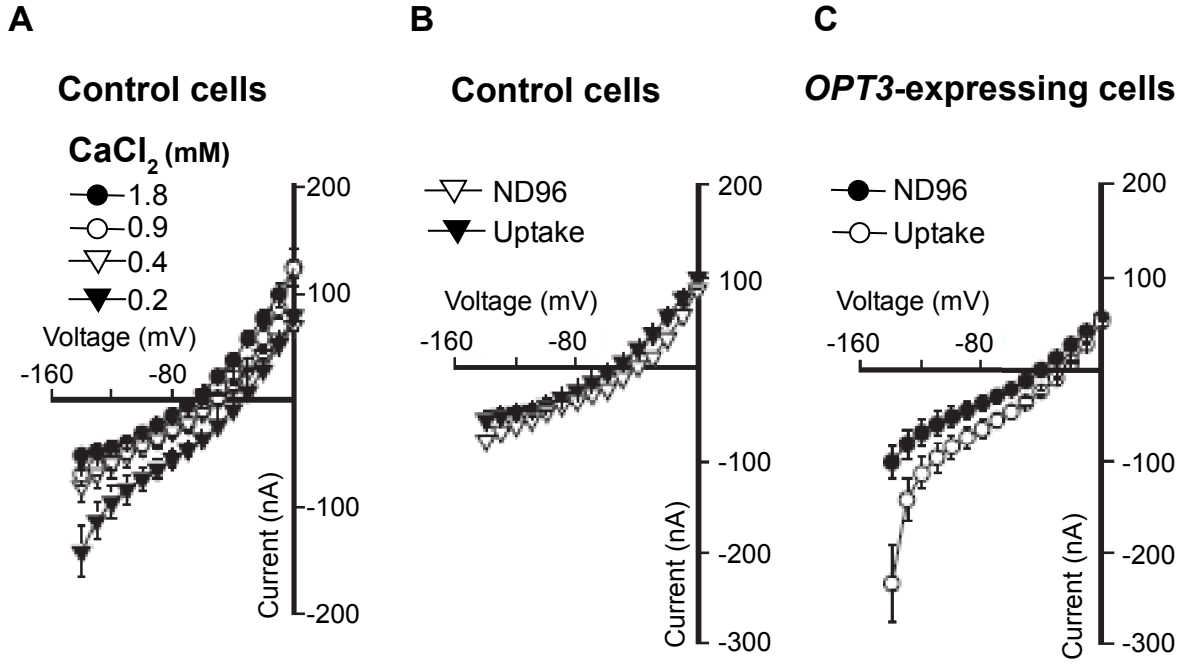

Supplemental Figure 4 online. Electrophysiological properties of *X. laevis* oocytes expressing *OPT3*. The mean current-voltage (***I/V***) curves shown were constructed from currents recorded in either water-injected control or *OPT3*-expressing cells elicited and measured as described in Figure 4. Notice the difference in the Y-axis magnitude between **A**, **B**, and **C**. **A.** Reducing extracellular Ca^{2+} from the ND96 recording solution results in increasingly inward current activity (i.e. negative currents) in control cells. The total $CaCl_2$ concentration present in the modified ND95 recording bath solutions are indicated in the legend. **B.** The electrical activity in control cells (i.e. endogenous currents in cells injected with water) is not altered in basal uptake solution (*i.e.* pH 6.0 and 0.9 mM $CaCl_2$) relative to that observed in ND96 recording solution. **C.** *OPT3*-expressing cells show an increase in inward current activity (i.e. negative currents) in basal uptake solution control cells relative to that observed in ND96 recording solution. Error bars represent S.E. (n=5).

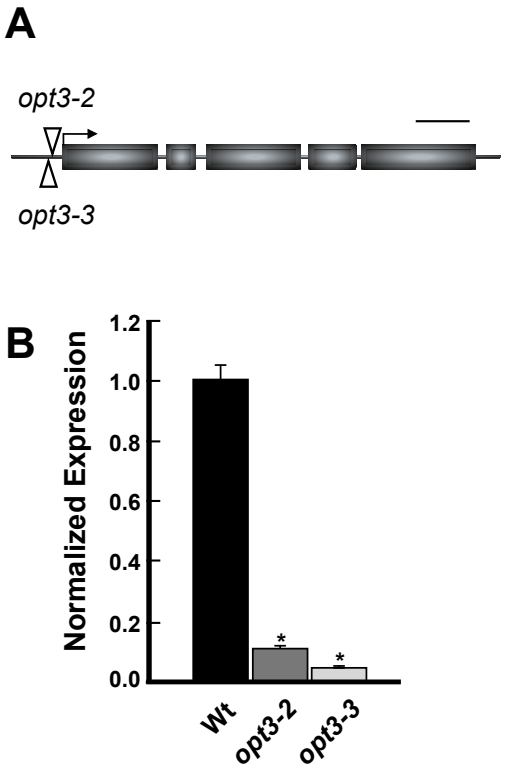

Supplemental Figure 5 online. T-DNA insertions upstream of the *OPT3* start codon reduce the *OPT3* transcript. A. The exon-intron structure of *OPT3*. Open arrowheads indicate T-DNA insertions located 36 and 41 bp upstream of start codon (black arrow) in *opt3-2* and *opt3-3* alleles, respectively. Bar = 500 bp. **B.** Transcript abundance of *OPT3* in wild-type (**Wt**) and *opt3-2* and *opt3-3* alleles (***opt3-2*** and ***opt3-3***, respectively). Expression of *OPT3* in mutant alleles is shown relative to its expression in Wt, which was set to 1. Shown are mean values ± S.E.; n = 9; asterisks (*) indicate statistically significant differences ($p \leq 0.001$) of *OPT3* transcript abundance in *opt3-2* or *opt3-3 vs*. Wt.

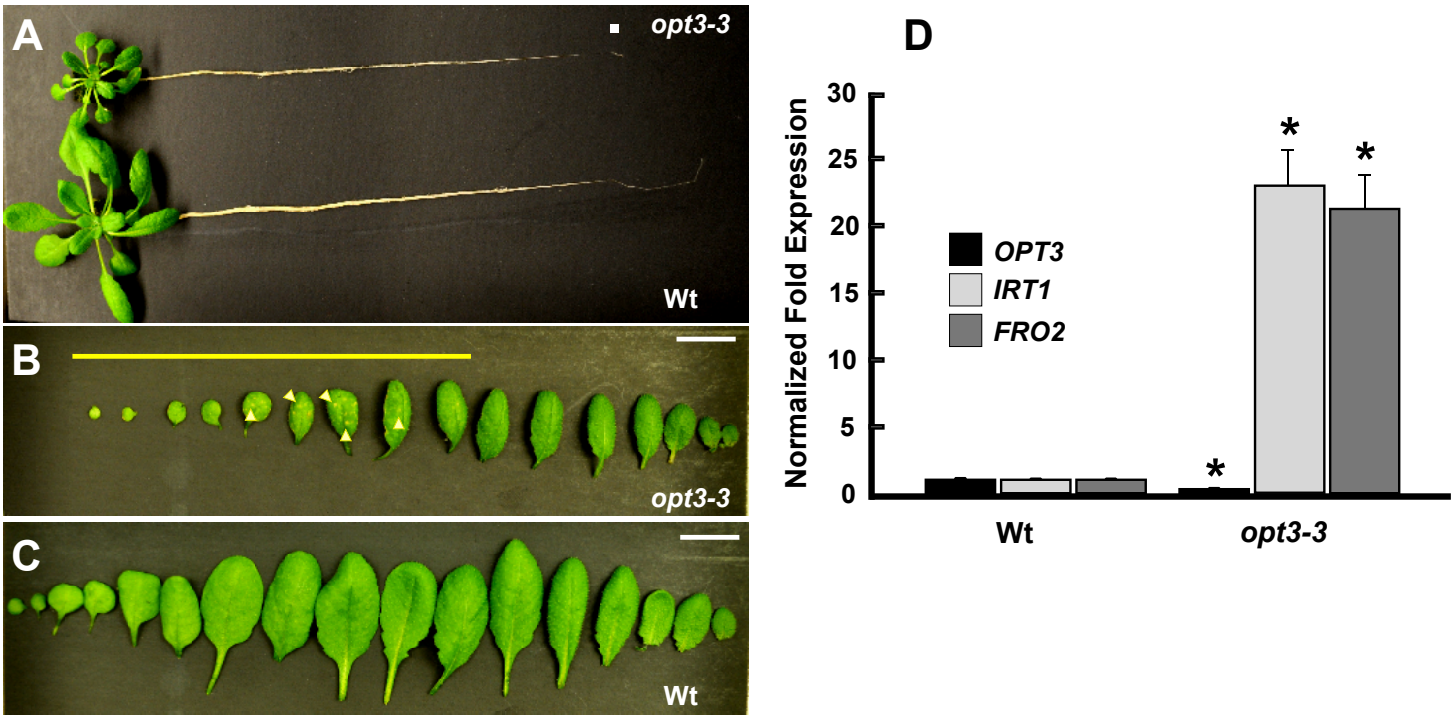

Supplemental Figure 6 online. The *opt3-3* knockdown allele (*opt3-3*) exhibits constitutive Fe deficiency symptoms. A. Representative images of hydroponically-grown wild-type and *opt3-3* plants are shown. **B.** Individual leaves of the *opt3-3* plant arranged from the oldest (left) to youngest (right) leaf. The yellow line shows older leaves with necrotic lesions (yellow arrows). **C.** Individual leaves of the wild-type plant, from oldest (left) to youngest (right). Bar = 1 cm. **D**. Quantitative real-time (qRT)-PCR analysis of the expression of Fe deficiency-responsive genes, *IRT1* and *FRO2,* in roots of wild-type (**Wt**) and *opt3-3* mutant (***opt3-3***) plants. Error bars indicate S.E. (n = 6). Asterisks (* $p \leq 0.05$) indicate statistically significant differences of transcript abundance of analyzed genes in *opt3-3 vs.* corresponding genes in wild-type, which were set to 1.

Supplemental Figure 7 online. Iron localizes at minor veins of old rosette leaves in the *opt3-3* mutant (*opt3-3*). Iron was localized using Perls' stain in plants grown hydroponically in Fe sufficient conditions until the late vegetative stage. Three old and young leaves were photographed from each plant line. Note the Fe staining in old leaves but not the young leaves of the *opt3-3* mutant. The lack of staining in young leaves of the *opt3-3* mutant and in all leaves of the wild-type (**Wt**) is due to low levels of Fe that are below the limit of detection. The inset shows that Fe is associated with minor veins of the *opt3-3* mutant.

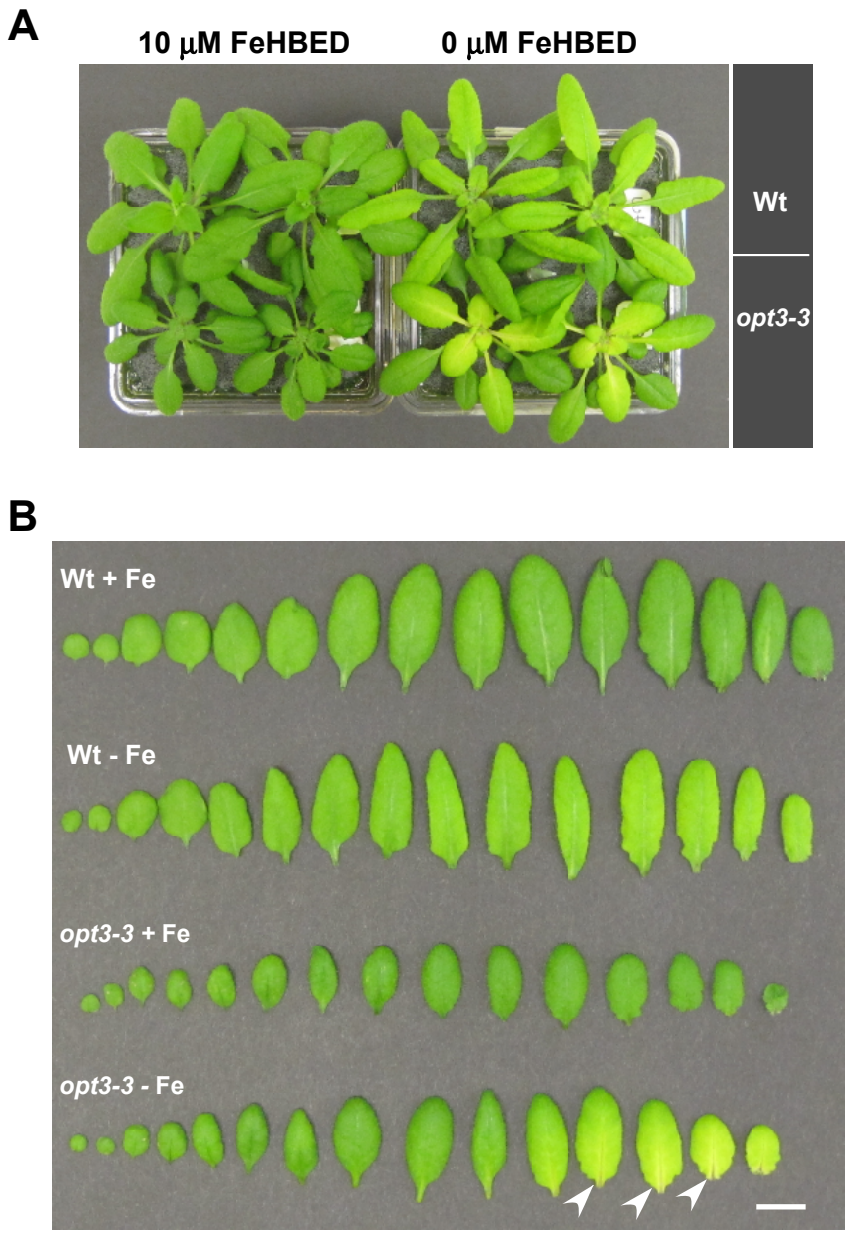

Supplemental Figure 8 online. Young leaves of the opt3-3 mutant are more sensitive to Fe deficiency than corresponding leaves of wild-type plants. A. Wild-type and *opt3-3* plants were grown hydroponically to the late vegetative stage before transferring to a fresh medium with (**10 μM FeHBED**) or without (**0 μM FeHBED**) 10 μM FeHBED. Plants were photographed after 7 days of subsequent growth **B.** Individual leaves of wild-type grown with or without 10 μM FeHBED (**Wt +Fe** and **Wt -Fe**, respectively) and *opt3-3* mutants grown with or without 10 μM FeHBED (***opt3-3* +Fe** and ***opt3-3* -Fe,** respectively) were arranged from the oldest (left) to youngest (right) leaf. Note that the youngest leaves of the *opt3-3* mutant are more chlorotic than the wild-type, especially at the midrib (arrows). Bar = 1 cm.

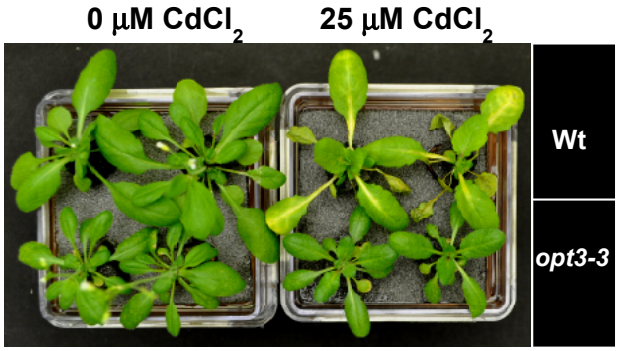

Supplemental Figure 9 online. Leaves of *opt3-3* mutant plants are less sensitive to Cd than leaves of wild-type. Wild-type **(Wt)** and *opt3-3* mutant plants **(*opt3-3*)** were grown grown hydroponicaly till the late vegetative stage and then treated with the indicated concentration of $CdCl_2$. Plants were photographed after 4 days of subsequent growth with Cd. Note that after exposure to 25 µM $CdCl_2$, leaves of wild-type plants wilted and developed chlorosis, while leaves of the *opt3-3* mutant did not show symptoms of Cd toxicity.

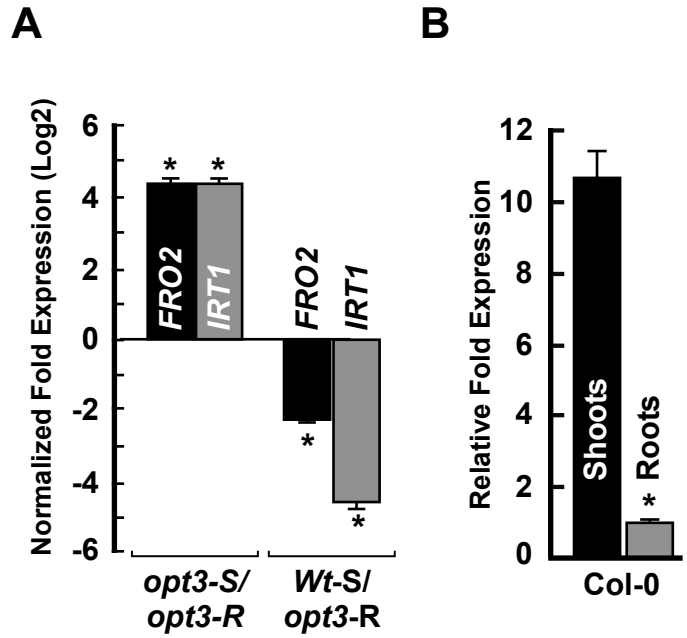

Supplemental Figure 10 online. OPT3 functions primarily in shoots in *A. thaliana*. A. Transcript abundance of *FRO2* and *IRT1* in roots of hydroponically grown the self-grafted *opt3-3* mutant **(*opt3-S/opt3-R*)** and reciprocally grafted plants with wild-type shoots and *opt3-3* roots (***Wt-S/opt3-R***). Data were normalized to the steady state level of *FRO2* and *IRT1* in roots of wild-type plants grown under identical conditions. **B**. The qRT-PCR analysis of the relative expression levels of *OPT3* in roots and leaves of wild-type plants. Mean values ± S.E. (n = 3) are shown. Asterisks indicate statistically significant differences (* $p \leq 0.05$).

Supplemental Table 1 online. Leaf element profile of wild-type (Wt) and the *opt3-3* (*opt3-3*) allele. Data represent the mean of 12 independent plants per genotype ± S.D. Data in bold represent elements with significant differences ($p \leq 0.05$) between *opt3-3* and wild type. The raw elemental concentrations for individual plant samples are available at www.ionomicshub.org in experimental tray1789 (Salk_058794). *ns*, not significant.

Element	Wild-type (µg g^{-1} Dry weight)	*opt3-3* (µg g^{-1} Dry weight)	Percentage Difference from the Wild Type	*P*-Values
Li	10.31±3.24	10.12±3.11	-2	Ns.
B	**97.38±9.37**	**71.25±7.13**	**-27**	**<0.0001**
Na	558.72±93.46	529.11±65.71	-5	ns
Mg	8507.89±589.40	8828.14±581.52	4	ns
P	8959.96±688.65	8778.49±873.51	-2	ns
K	**45192.01±3937.93**	**34799.39±4059.54**	**-23**	**<0.0001**
Ca	33529.96±2438.29	32300.06±3020.20	-4	ns
Mn	**59.08±27.74**	**158.43±48.21**	**168**	**<0.0001**
Co	**0.52±0.11**	**1.77±0.28**	**241**	**<0.0001**
Ni	1.00±0.10	1.12±0.15	12	ns
Cu	**7.92±2.02**	**10.43±2.11**	**32**	**0.0014**
Zn	**115.77±81.87**	**240.83±82.70**	**108**	**0.0006**
As	0.88±0.33	0.80±0.30	-9	ns
S	**11415.58±1525.68**	**9676.14±1129.73**	**-15**	**0.005**
Fe	**101.88±6.83**	**213.53±25.54**	**110**	**<0.0001**
Se	8.64±3.18	8.74±2.36	1	ns
Rb	**83.74±15.43**	**68.79±11.26**	**-18**	**0.008**
Sr	67.03±8.23	66.75±6.08	0	ns
Mo	**28.65±1.86**	**24.97±3.08**	**-13**	**0.0004**
Cd	**0.64±0.089**	**1.10±0.13**	**72**	**<0.0001**

Supplemental Table 2 online. **List of oligos.** Nucleotide sequence marked in bold indicate *att* sites.

Name	**Sequence**	**Purpose**
LBb1.3	ATTTTGCCGATTTCGGAAC	genotyping
Fopt3-2	CAAAATCCATTCGGACATGTC	genotyping
Ropt3-2	GAGGCTAAAACTCCACCCAAG	genotyping
Fopt3-3	CGGACAACCAATAGAAAGTGC	genotyping
Ropt3-3	GAGAAGTGGTGGGAAGAGTCC	genotyping
Fcad1-3	AATTGCAGACTGGGACTGGT	genotyping
Rcad13dCAP	CTTCCCAAAGAAGTTTAAGAGGGAT	genotyping
FOPT3	**TCGTCGGGGACAACTTTGTACAAAAAAGTTGG**TCAGAATCTCCAATCCTACTCTCC	complementation in the *opt3-3* mutant
ROPT3	**GGCGGCCGCACAACTTTGTACAAGAAAGTTGGGT**TGATGCAATTCCAATGGGTAG	complementation in the *opt3-3* mutant
FOPT3pro	**TCGTCGGGGACAACTTTGTACAAAAAAGTTGG**GGTCCAGTAGGCCATTTCACAT	GUS activity
ROPT3pro	**GGCGGCCGCACAACTTTGTACAAGAAAGTTGGGT**CTGGCAGAAAGTGAATGCTGTT	GUS activity
FOPT3-CDS	**TCGTCGGGGACAACTTTGTACAAAAAAGTTGG**GAAAATGGACGCGGAGAAG	cloning in YES3-Gate and GWB406
ROPT3-CDS*	**GGCGGCCGCACAACTTTGTACAAGAAAGTTGGGT**TTAGAAAACGGGACAGCCTTT	complementation in *opt1*Δ and *opt2*Δ yeast
ROPT3-CDS	**GGCGGCCGCACAACTTTGTACAAGAAAGTTGGGT**GAAAACGGGACAGCCTTTGG	complementation in *opt1* Δ and *opt2*Δ yeast
FOPT3	CTCTTCATCGTCTTGACCACTC	qRT-PCR
ROPT3	ACTTGTTTTCCTTCTCGTGC	qRT-PCR
FF14F8.90	TTTCGGCTGAGAGGTTCGAGT	qRT-PCR
RF14F8.90	GATTCCAAGACGTAAAGCAGATCAA	qRT-PCR
FFIT1	AGAACATGCTCCTGATGCTC	qRT-PCR
RFIT1	CACACCAATCTCACATAAAACCC	qRT-PCR

FIRT1	ACCCGTGCGTCAACAAAGCTAAAG	qRT-PCR
RIRT1	TCCCGGAGGCGAAACACTTAATGA	qRT-PCR
FFRO2	TGTGGCTCTTCTTCTCTGGTGCTT	qRT-PCR
RFRO2	TGCCACAAAGATTCGTCATGTGCG	qRT-PCR
FHMA2	TCAGGGTGTTGTGGTGACAAGAGT	qRT-PCR
RHMA2	TCCAGGCCAGATGGCTTGTTATGA	qRT-PCR
FHMA4	GAACCGCAGCCCAAATCAAAGGAT	qRT-PCR
RHMA4	GGCTCTGCTCTTGCAACACAAACT	qRT-PCR
FFPN2	ACGAGTTCTGAACACCTCCAACCA	qRT-PCR
RFPN2	TCATGGCTGGAGTTGCTGCTTCTA	qRT-PCR
FCAX2	AGACGGCGATGCTGTTCATC	qRT-PCR
RCAX2	GTGTACAAAGAAACTGGCAGCTAC	qRT-PCR
FCAX4	GCTTGTTTTGCCTTGTCCATTC	qRT-PCR
RCAX4	GGGTGAGTTAGAGACAAAGAAGC	qRT-PCR
FABCC1	AGAGCGTTGGTGGCCATCTCTTTA	qRT-PCR
RABCC1	GTGTTGCATTCTGTTCCTCGCCAA	qRT-PCR
FABCC2	TCTAGAGAGGGATGGTTGTCA	qRT-PCR
RABCC2	CATTCGGTTCCTTGCCAATC	qRT-PCR
FMTP3	CTTAATCGAGCAAAAGAAGCAGC	qRT-PCR
RMTP3	CCACTCCGGCTTATACCATATG	qRT-PCR
FACT2	GACCTTTAACTCTCCCGCTA	qRT-PCR
RACT2	GGAAGAGAGAAACCCTCGTA	qRT-PCR

Supplemental Methods Online

In vitro GSH Uptake

S. cerevisiae opt1 mutant cells transformed with YES3-Gate-ScOPT1, YES3-Gate-At-OPT3 or the empty YES3-Gate vector were grown in YNB-URA to OD_{600} = 0.8. Uptake studies were performed using modified procedures of (Pence *et al.*, 2000, Zhang *et al.*, 2004). Briefly, cells were harvested by centrifugation, washed from the culture medium with deionized water and a washing buffer containing 20 mM MES/KOH, 50 μM $CaCl_2$ and 25 μM $MgCl_2$, pH 5.0, before re-suspension in the ice-cold uptake buffer (washing buffer supplemented with 2% [w/v] glucose), all solutions were kept on ice. After warming to room temperature, cells were mixed with equal volumes of radiolabeled [^{35}S] GSH (100 μM, specific activity 30 Ci/mmol) and incubated at room temperature for the indicated time points. [^{35}S] GSH radioactivity was measured in yeast pellets obtained after centrifugation of 100 μl cell suspension aliquots through a silicone oil/dionyl phthalate mixture onto 10 μl of 40% perchloric acid (Pence *et al.*, 2000).

Expression of the *OPT3-EGFP* Chimera in *Xenopus* Oocytes

The T7TS vector was used as the backbone to generate the *OPT3-EGFP* chimera. First, the *EGFP* ORF was amplified using a 5′ end adaptor consisting of an *SpeI* adaptor followed by a short linker sequence (TSGG) immediately upstream of the *EGFP* coding region (initiation codon removed). The 3′ end adaptor consisted of an additional stop codon downstream of the *EGFP* stop codon, followed by a *SpeI* adaptor. The resulting product was cloned into the *SpeI* site of the T7TS plasmid. This backbone plasmid was named T7TS-C-EGFP. The ORF of *OPT3* without a stop codon was amplified using EcoRV adaptors, and cloned into the EcoRV site of the T7TS-C-EGFP vector, resulting in an *OPT3-EGFP* chimera joint by a DITSTSGG linker.

Synchrotron X-ray fluorescence microscopy (SXRF)

Wild-type and *opt3-3* mutant plants were grown on solid ½ MS medium for 23 days. Fully developed leaves (2nd from the bottom) were detached immediately prior analysis using Teflon-

coated forceps and placed, adaxial side uppermost, on 35 mm slide mounts across which Kapton™ metal-free tape was stretched. The distribution of Fe in hydrated leaf tissue was imaged *via* SXRF at hard X-ray microprobe X26A of the National Synchrotron Light Source. This is a bending magnet beamline, which uses Kirkpatrick-Baez focusing optics. Photon Flux at 18 keV is approximately $1x10^9$ photons/sec in focused monochromatic mode, which causes no discernible beam damage to hydrated plant samples. The microprobe is equipped with a Canberra 9-element HPGe Array detector, and two Radiant Vortex-EX Silicon Drift Diode (SDD) detectors, providing trace element analyses detection with 1≈ ppm sensitivity. Leaves were raster scanned in 6 µm steps the x and y directions to provide the Fe map. A focused, monochromatic incident X-ray beam of 11 keV, and dimensions of 7 x 10 µm was used for leaf analysis, with dwell times of 0.25 second/pixel. Each leaf sample took approximately 6 hours to image from petiole to hydathode. Quantification of fluorescence counts into µg cm^{-1} used a standards-based approached as described previously (Punshon *et al.*, 2013).

Supplemental References Online

Amasheh, S. and Weber, W. (1999) Further characteristics of the Ca^{2+}-inactivated Cl^- channel in *Xenopus laevis* oocytes. *J Membr Biol*, **172**, 169-179.

Gayomba, S.R., Jung, H.I., Yan, J., Danku, J., Rutzke, M.A., Bernal, M., & Vatamaniuk, O.K. (2013) The CTR/COPT-dependent copper uptake and SPL7-dependent copper deficiency responses are required for basal cadmium tolerance in *A. thaliana*. *Metallomics*, **5**, 1262-1275.

Jung, H.I., Gayomba, S.R., Rutzke, M.A., Craft, E., Kochian, L.V. and Vatamaniuk, O.K. (2012) COPT6 is a Plasma Membrane Transporter that Functions in Copper Homeostasis in *Arabidopsis* and is a Novel Target of SQUAMOSA Promoter Binding Protein-Like 7. *J Biol Chem*, **287**, 33252-33267.

Kuruma, A., Hirayama, Y. and Hartzell, H.C. (2000) A hyperpolarization- and acid-activated nonselective cation current in Xenopus oocytes. *Am J Physiol Cell Physiol*, **279**, C1401-1413.

Pence, N.S., Larsen, P.B., Ebbs, S.D., Letham, D.L., Lasat, M.M., Garvin, D.F., & Kochian, L.V. (2000) The molecular physiology of heavy metal transport in the Zn/Cd hyperaccumulator *Thlaspi caerulescens*. *Proc Natl Acad Sci USA*, **97**, 4956-4960.

Pfaffl, M.W., Horgan, G.W. and Dempfle, L. (2002) Relative expression software tool (REST) for group-wise comparison and statistical analysis of relative expression results in real-time PCR. *Nucleic Acids Res*, **30**, e36.

Punshon, T., Ricachenevsky, F.K., Hindt, M.N., Socha, A.L. and Zuber, H. (2013) Methodological approaches for using synchrotron X-ray fluorescence (SXRF) imaging as a tool in ionomics: examples from *Arabidopsis thaliana*. *Metallomics*, **5**, 1133-1145.

Rus, A., Baxter, I., Muthukumar, B., Gustin, J., Lahner, B., Yakubova, E. and Salt, D.E. (2006) Natural variants of AtHKT1 enhance Na+ accumulation in two wild Populations of Arabidopsis. *Plos Genet*, **2**, 1964-1973.

Zhang, M.-Y., Bourbouloux, A., Cagnac, O., Srikanth, C.V., Rentsch, D., Bachhawat, A.K. and Delrot, S. (2004) A Novel Family of Transporters Mediating the Transport of Glutathione Derivatives in Plants. *Plant Physiol.*, **134**, 482-491.